Global Landscape and Regulatory Principles of DNA Methylation Reprogramming for Germ Cell Specification by Mouse Pluripotent Stem Cells

白根, 健次郎

https://doi.org/10.15017/1806892

出版情報：九州大学, 2016, 博士（医学）, 課程博士
バージョン：
権利関係：全文ファイル公表済

Resource

Developmental Cell

Global Landscape and Regulatory Principles of DNA Methylation Reprogramming for Germ Cell Specification by Mouse Pluripotent Stem Cells

Graphical Abstract

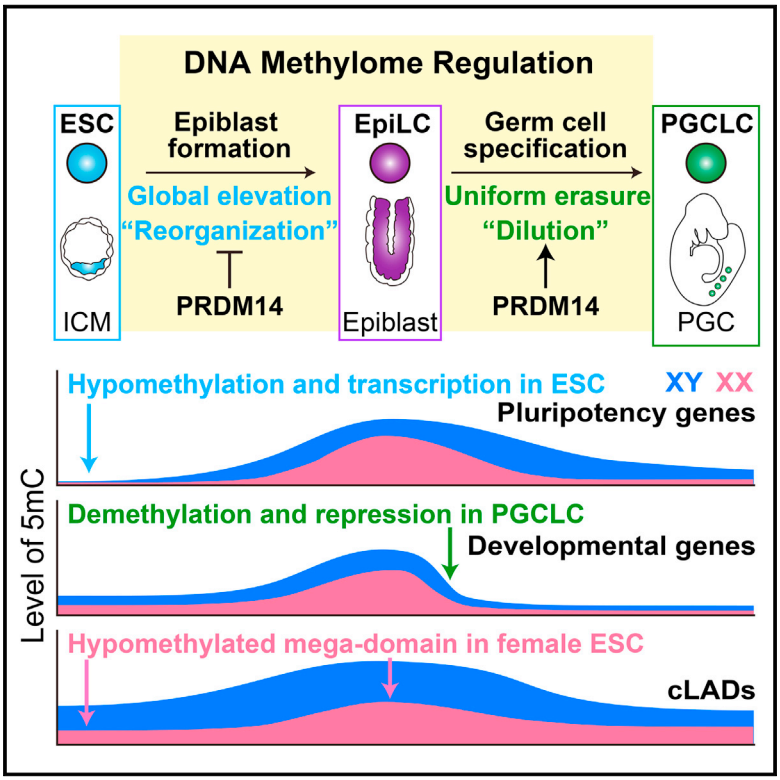

Highlights

- In vitro primordial germ cell specification from mouse ESCs models in vivo process
- PGCLC methylome is derived from progressive dilution of epiblast-like cell methylome
- PRDM14 differentially impacts the hypomethylation in ESCs and PGCLCs
- Female ESCs, but not PGCLCs, create hypomethylated lamina-associated domains

Authors

Kenjiro Shirane, Kazuki Kurimoto, Yukihiro Yabuta, ..., Katsuhiko Hayashi, Mitinori Saitou, Hiroyuki Sasaki

Correspondence

saitou@anat2.med.kyoto-u.ac.jp (M.S.), hsasaki@bioreg.kyushu-u.ac.jp (H.S.)

In Brief

DNA methylation reprogramming is important for germ cell development and embryogenesis. Shirane et al. constructed DNA methylation maps of mouse primordial germ cell (PGC)-like cells, produced from embryonic stem-cell-derived epiblast-like cells, as a model of PGC specification. These analyses suggest distinct methylation regulation in stem cells versus germ cells.

Accession Numbers

DRA003471

Shirane et al., 2016, Developmental Cell *39*, 87–103
October 10, 2016
http://dx.doi.org/10.1016/j.devcel.2016.08.008

CellPress

Developmental Cell
Resource

Global Landscape and Regulatory Principles of DNA Methylation Reprogramming for Germ Cell Specification by Mouse Pluripotent Stem Cells

Kenjiro Shirane,[1,2] Kazuki Kurimoto,[3,4] Yukihiro Yabuta,[3,4] Masashi Yamaji,[3,4,10] Junko Satoh,[5] Shinji Ito,[5] Akira Watanabe,[6,7] Katsuhiko Hayashi,[3,8,9] Mitinori Saitou,[3,4,6,7,*] and Hiroyuki Sasaki[1,11,*]

[1]Division of Epigenomics and Development, Medical Institute of Bioregulation, and Epigenome Network Research Center, Kyushu University, Maidashi 3-1-1, Higashi-ku, Fukuoka 812-8582, Japan

[2]Graduate School of Medical Sciences, Kyushu University, Maidashi 3-1-1, Higashi-ku, Fukuoka 812-8582, Japan

[3]Department of Anatomy and Cell Biology, Graduate School of Medicine, Kyoto University, Yoshida-Konoe-cho, Sakyo-ku, Kyoto 606-8501, Japan

[4]JST, ERATO, Yoshida-Konoe-cho, Sakyo-ku, Kyoto 606-8501, Japan

[5]Medical Research Support Center, Graduate School of Medicine, Kyoto University, Yoshida-Konoe-cho, Sakyo-ku, Kyoto 606-8501, Japan

[6]Center for iPS Cell Research and Application, Kyoto University, 53 Kawahara-cho, Shogoin, Sakyo-ku, Kyoto 606-8507, Japan

[7]Institute for Integrated Cell-Material Sciences, Kyoto University, Yoshida-Ushinomiya-cho, Sakyo-ku, Kyoto 606-8501, Japan

[8]Department of Developmental Stem Cell Biology, Faculty of Medical Sciences, Kyushu University, Maidashi 3-1-1, Higashi-ku, Fukuoka 812-8582, Japan

[9]JST, PRESTO, Maidashi 3-1-1, Higashi-ku, Fukuoka 812-8582, Japan

[10]Present address: Howard Hughes Medical Institute, Laboratory of RNA Molecular Biology, The Rockefeller University, 1230 York Avenue, Box #186, New York, NY 10065-6399, USA

[11]Lead Contact

*Correspondence: saitou@anat2.med.kyoto-u.ac.jp (M.S.), hsasaki@bioreg.kyushu-u.ac.jp (H.S.)

http://dx.doi.org/10.1016/j.devcel.2016.08.008

SUMMARY

Specification of primordial germ cells (PGCs) activates epigenetic reprogramming for totipotency, the elucidation of which remains a fundamental challenge. Here, we uncover regulatory principles for DNA methylation reprogramming during in vitro PGC specification, in which mouse embryonic stem cells (ESCs) are induced into epiblast-like cells (EpiLCs) and then PGC-like cells (PGCLCs). While ESCs reorganize their methylome to form EpiLCs, PGCLCs essentially dilute the EpiLC methylome at constant, yet different, rates between unique sequence regions and repeats. ESCs form hypomethylated domains around pluripotency regulators for their activation, whereas PGCLCs create demethylation-sensitive domains around developmental regulators by accumulating abundant H3K27me3 for their repression. Loss of PRDM14 globally upregulates methylation and diminishes the hypomethylated domains, but it preserves demethylation-sensitive domains. Notably, female ESCs form hypomethylated lamina-associated domains, while female PGCLCs effectively reverse such states into a more normal configuration. Our findings illuminate the unique orchestration of DNA methylation and histone modification reprogramming during PGC specification.

INTRODUCTION

Epigenetic reprogramming of the developmental potency during the germline cycle is vital for ensuring a continuous generation of totipotent zygotes (Lee et al., 2014; Saitou et al., 2012; Sasaki and Matsui, 2008). Key reprogramming events that occur during specification and development of primordial germ cells (PGCs) include global DNA demethylation as well as histone modification reprogramming. Recent studies showed that, after the specification period, PGCs at embryonic day 9.5 (E9.5) or later undergo replication-coupled passive demethylation, compensated by an active mechanism acting on specific loci (Arand et al., 2015; Gkountela et al., 2015; Guo et al., 2015; Hackett et al., 2013; Kagiwada et al., 2013; Kobayashi et al., 2013; Seisenberger et al., 2012; Tang et al., 2015; Yamaguchi et al., 2013). However, questions arise as to the mechanism that directs epigenetic reprogramming during PGC specification, relationships between the changes in DNA methylation and histone modifications, differences in the epigenome regulation between PGCs, their precursors, and pluripotent stem cells, and the impact of epigenetic reprogramming on subsequent gametogenesis. Systematic exploration of such issues has been difficult, due to the limited amount of materials available from PGCs and the lack of an in vitro system that recapitulates germ cell development.

Recent studies showed that mouse epiblast-like cells (EpiLCs) induced from pluripotent stem cells (i.e., embryonic stem cells [ESCs] and induced pluripotent stem cells [iPSCs]) cultured in the presence of inhibitors of the mitogen-activated protein kinase pathway (MEKi) and the glycogen synthase kinase 3 pathway (GSK3i), known as 2i (Ying et al., 2008), can be further induced into primordial germ cell-like cells (PGCLCs), which

show robust capacity for spermatogenesis and oogenesis (Hayashi et al., 2011, 2012). This PGCLC induction system has also been demonstrated as a precise reconstitution of PGC specification by the proper reprogramming of the gene-expression profile (Hayashi et al., 2011, 2012). Accordingly, the PGCLC induction system has been exploited for identification of transcription factors involved in PGC induction (Murakami et al., 2016; Nakaki et al., 2013), clarification of signaling mechanisms for PGC specification (Aramaki et al., 2013), and, more recently, development of a PGCLC induction system in human ESCs and iPSCs, which provides a foundation for understanding and reconstituting human germ cell development in vitro (Irie et al., 2015; Sasaki et al., 2015).

Using the mouse PGCLC induction system, we recently reported large-scale histone modification reprogramming during PGC specification and a potential mechanism for this reprogramming (Kurimoto et al., 2015). Here, using the same system, we study the comprehensive picture of the dynamic DNA methylation reprogramming that occurs during PGC specification and its relationship with the histone modification reprogramming.

RESULTS

Design of the Study

At the outset, we determined the levels of unmodified cytosine (C), 5-methylcytosine (5mC), and 5-hydroxymethylcytosine (5hmC) (Kriaucionis and Heintz, 2009; Tahiliani et al., 2009) in key cell types of the mouse PGCLC induction system (male ESCs, EpiLCs, and day-6 [d6] PGCLCs [*Blimp1-mVenus*-positive cells; Hayashi et al., 2011]) by mass spectrometry (MS) and whole-genome bisulfite sequencing (WGBS) (Figure 1 and Table S1). The MS analysis revealed a rapid increase in 5mC level upon transition from ESC to EpiLC, followed by an acute decrease during PGCLC induction (Figure 1B). In contrast, the 5hmC level remained very low (1%–3% of 5mC level) in all cell types (Figure 1B). The results from the WGBS were essentially identical to those obtained by MS (Figure 1C and Table S1). Furthermore, biological replicates showed excellent reproducibility in WGBS (Figures 1C and 1D; Table S1) and, therefore, we performed more detailed WGBS data analysis in single replicates (Figure 1D and Table S1). Since the 5hmC level was negligible (Figure 1B), and since bisulfite sequencing does not distinguish 5mC from 5hmC (Hayatsu and Shiragami, 1979), we describe both modified bases as 5mC in this study. We focused on the 5mCs in CpG contexts, since CpH (where H = A, C, or T) methylation was limited in these cells (Figure 1C and Table S1) and had no known biological role in mammalian cells (Schubeler, 2015). We also analyzed the transcriptomes of all cell types by RNA sequencing (RNA-seq) (Table S2).

As a key parameter for the global DNA methylation state, we determined the average 5mC level of the total unique sequence regions (unique regions; in 2-kb windows with 1-kb overlaps). We separately determined the 5mC levels of the promoters (divided into high [HCPs], intermediate [ICPs], and low CpG density promoters [LCPs]) (Weber et al., 2007), consensus sequences of the repeat elements (long interspersed nuclear element 1 [LINE1]; intracisternal A particle [IAP]; endogenous retroviruses [ERVs] other than IAP; major and minor satellites) (Table S3), and imprint control regions (ICRs) associated with the imprinted genes. We also determined the 5mC levels of non-promoter CpG islands (CGIs) (Illingworth et al., 2010), exons, introns, intergenic regions, cell-specific enhancers (Kurimoto et al., 2015), and evolutionarily young short interspersed nuclear elements B1 (SINE B1) (Table S3).

EpiLCs Reorganize the ESC Methylome

We first characterized the methylome of ESCs derived and cultured in 2i in comparison with that of the inner cell mass (ICM) of E3.5 blastocysts. We used an MEKi concentration of 0.4 μM instead of the original 1 μM (Ying et al., 2008), since ESCs cultured with this concentration of MEKi adhere to dishes more efficiently and serve as a more suitable source for EpiLC induction (Hayashi et al., 2011). When published data of the ICM (Wang et al., 2014) was reprocessed, low 5mC levels were evident in the unique regions (average 23%) and all three classes of promoters (Figure S1A). Published data from ESCs cultured with 1 μM MEKi (Habibi et al., 2013) revealed a global 5mC level similar to that of the ICM (21%) with smaller variations (Figures S1A and S1B). In contrast, ESCs cultured with 0.4 μM MEKi showed higher 5mC levels in the unique regions (58%) and promoters (particularly ICPs and LCPs), but not in the repeats, than those cultured with 1 μM MEKi and the ICM (Figures S1A and S1B). Notably, the 5mC distributions in the unique regions and promoters (and to a lesser extent, in the repeats) were divergent between ESCs and the ICM (Figures S1B and S1C). These findings highlight the differences between the ESC and ICM methylomes and the key role of MEKi in decreasing the global 5mC level in a dose-dependent fashion. It is notable that the repeats generally show relatively constant 5mC levels (Figure S1B).

The ESC-to-EpiLC transition resulted in an increase in 5mC level in the unique regions (from 58% to 73%) and promoters (particularly the ICPs and LCPs), but not the repeats, and consequently, EpiLCs acquired a methylome highly similar to that of the epiblast at E6.5 (70%) (Seisenberger et al., 2012) (Figures S1A–S1C and Table S1). The increase observed during this transition was not even, with the unique regions and promoters of the 10%–75% 5mC range showing a greater increase, indicating significant methylome reorganization (Figure S1B). We compared the methylome of EpiLCs with that of neural progenitor cells (NPCs) induced from ESCs (Stadler et al., 2011) and found that NPCs show higher 5mC levels in the unique regions (average 85%) and many promoters (Figures S1A and S1B; Table S1). Thus, EpiLCs had a 5mC level intermediate between ESCs and NPCs, recapitulating the state of the epiblast, which is intermediate between the ICM and somatic tissues (Wang et al., 2014). Collectively, EpiLCs recapitulate the methylome of the epiblast, which probably represents an epigenome appropriate for differentiation toward somatic lineages (higher 5mC level) as well as the germ cell lineage (lower 5mC level).

PGCLCs Progressively Dilute the EpiLC Methylome

The high similarity between the EpiLC and epiblast methylomes suggests that the EpiLC methylome would give an appropriate reference for DNA methylation changes that occur during PGCLC specification. The PGCLC induction from EpiLCs resulted in a decrease in 5mC level in essentially all genomic regions (Figures 2A, 2B, and S2A). The methylome of d2 PGCLCs

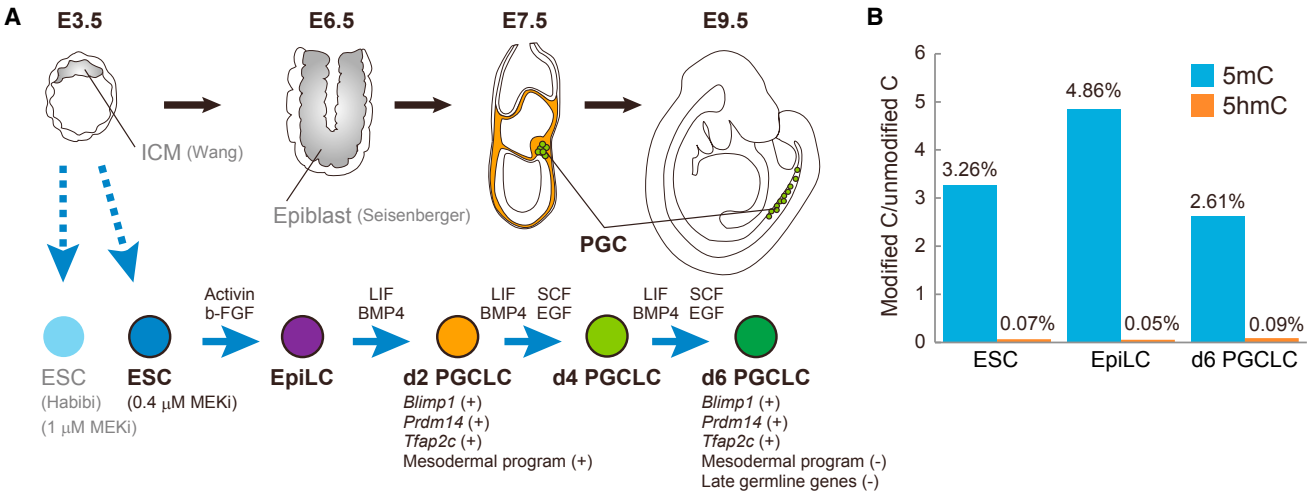

D

Cell type	Sample name	Total sequence (Gb)	Genome coverage	%CpG covered	Average %CpG methylation	
ESC	Male rep1	76.3	14.0	97.4	57.9	*R* = 0.91
	Male rep2	116.3	27.3	93.1	51.3	
	Male *Prdm14* KO	89.8	13.4	96.6	75.7	
	Female	100.7	22.6	92.8	21.2	
EpiLC	Male rep1	67.0	11.7	96.5	73.4	*R* = 0.92
	Male rep2	94.8	22.5	92.8	76.8	
	Male *Prdm14* KO	87.9	14.5	97.0	81.5	
	Female	100.9	22.8	92.7	64.1	
d2 PGCLC	Male rep1	71.3	14.2	97.5	71.9	
	Male *Prdm14* KO	104.6	17.2	97.4	81.0	
d4 PGCLC	Male rep1	105.2	21.7	98.1	50.0	
	Male *Prdm14* KO	72.7	14.9	97.4	75.2	
d6 PGCLC	Male rep1	97.6	19.9	98.0	37.3	*R* = 0.83
	Male rep2	101.9	25.3	92.9	39.1	
	Male *Prdm14* KO	114.5	23.5	98.2	68.4	
	Female	101.9	22.0	92.8	16.2	

Figure 1. Design and Summary of WGBS

(A) Schematic representation of PGC specification and PGCLC induction.

(B) Levels of 5mC (blue) and 5hmC (orange) relative to unmodified C determined by MS. The average values from two independent experiments are shown.

(C) Fractions of 5mCs present in the respective dinucleotide context determined by WGBS. The results from biological replicates are shown separately. Color coding is as indicated.

(D) Summary of the WGBS.

was still similar to that of EpiLCs, but demethylation proceeded steadily during continued culture (37% in d6 PGCLCs), while still preserving the 5mC distribution pattern established in EpiLCs (Figure 2B). The rate of demethylation was greater in the unique regions and promoters than in the repeats. Consequently, d6 PGCLCs showed about half the 5mC levels of EpiLCs in the unique regions and promoters (0.46- and 0.49-fold, respectively), and a 0.78-fold level in the repeats (Figure 2B). The degree of demethylation was relatively constant in the respective categories (Figure S2B). Thus, the global demethylation that occurs upon PGCLC induction is essentially a dilution of the EpiLC methylome with different kinetics for the unique regions/promoters and repeats.

We next examined the demethylation kinetics of individual genomic elements during PGCLC induction. Similar 5mC levels and demethylation kinetics were observed for the LCPs, exons, introns, and intergenic regions, which were essentially identical to those for the unique regions (Figures 2C and 2D). The HCPs, ICPs, non-promoter CGIs, and cell-specific enhancers had lower 5mC levels (Figures 2C and S2C) and, among them, the non-promoter CGIs and some cell-specific enhancers showed different 5mC dynamics (Figures 2D and S2C). Thus, the ESC- and EpiLC-specific enhancers, marked by histone H3 lysine-27 acetylation (H3K27ac) in the respective cell types (Kurimoto et al., 2015), showed an initial small increase and a subsequent decrease in 5mC level upon PGCLC induction. In contrast, the d2 and d6 PGCLC-specific enhancers showed demethylation kinetics similar to those of the unique regions (Figures 2C, 2D, and S2C). Among the repeats and ICRs, IAPs, LINE1s, the maternally methylated ICRs, and the major and minor satellites showed

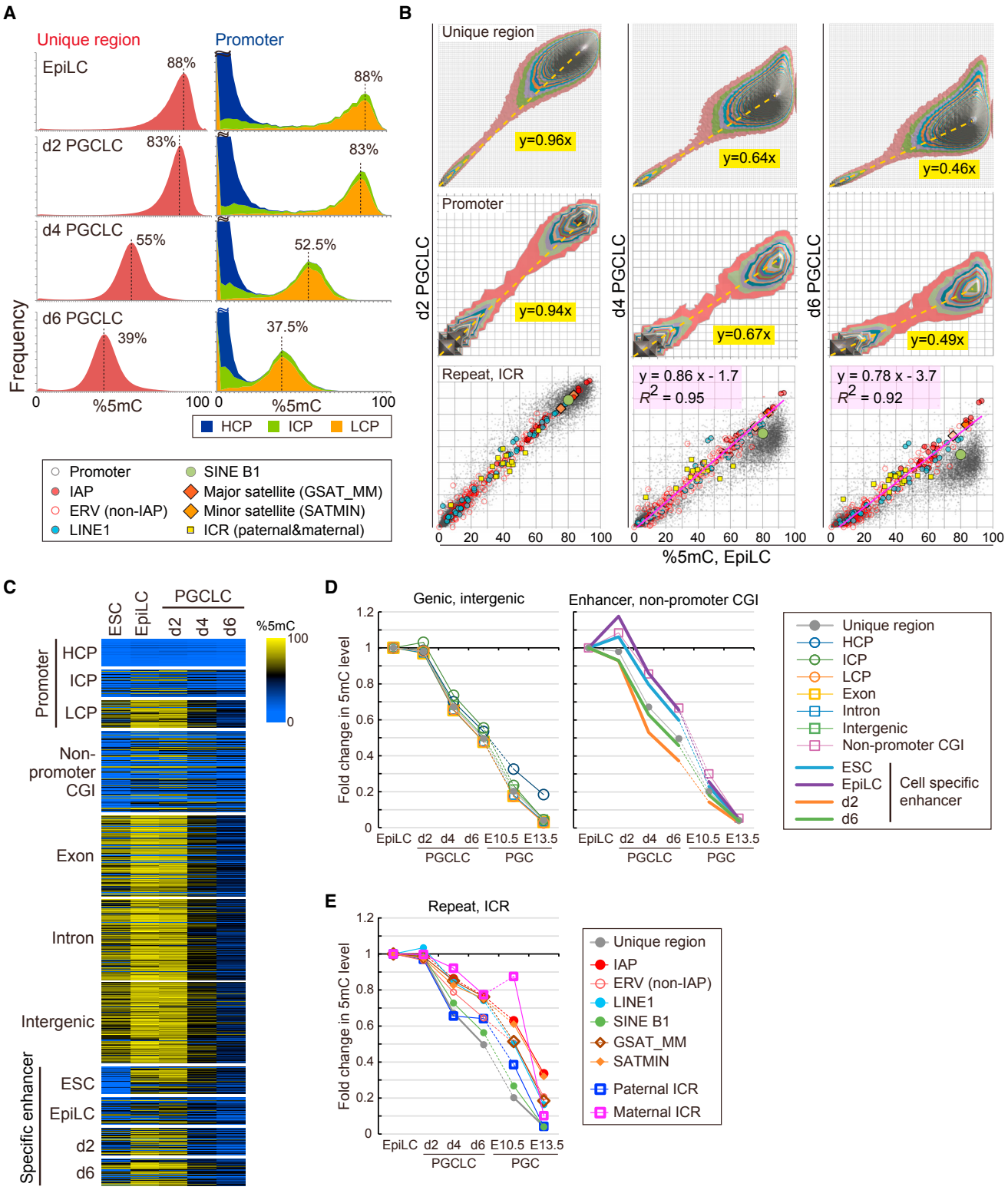

Figure 2. PGCLCs Dilute the EpiLC Methylome

(A) Histograms showing the distributions of the unique regions (2-kb windows) (left) and promoters (right) across 5mC levels in indicated cells. The mode 5mC level is indicated for the unique regions and LCPs. Color coding is as indicated.

(B) Comparisons of the 5mC levels of indicated genomic elements between indicated cells. Contour-plot (for the unique regions [2-kb windows] and promoters) (top and middle) or scatterplot representation (for the repeats and ICRs) (bottom) is used. Contour lines are drawn with an interval of 100 windows or 25 promoters.

(legend continued on next page)

slower and lesser demethylation (Figure 2E). ERVs other than IAPs and the paternally methylated ICRs showed a demethylation rate intermediate between the above repeats and unique regions (Figure 2E). Among the paternally methylated ICRs, the *H19* and *Rasgrf1* ICRs showed faster demethylation than the *Dlk1-Gtl2* ICR (Figure S2D).

Consistent with the notion that d6 PGCLCs correspond to E9.5 PGCs in vivo (Hayashi et al., 2011) and that developing PGCs have a progressively lower 5mC level, the level was lower in E10.5 and E13.5 PGCs (Kobayashi et al., 2013) than in d6 PGCLCs (Figures 2D, 2E, S2E, and S2F; Table S1). Importantly, the 5mC distribution patterns were highly similar between d6 PGCLCs and E10.5 PGCs (Figure S2F), indicating that E10.5 PGCs have a methylome corresponding to a diluted state of the d6 PGCLC methylome. These results further demonstrate the precise recapitulation of PGC specification and development by the PGCLC induction system.

ESCs and PGCLCs Show Distinct Correlations between DNA Hypomethylation, Histone Modification, and Gene Expression

Next, we wanted to correlate the changes in DNA methylation, histone modifications, and gene transcription in ESCs and PGCLCs. To this end, we identified regions (2-kb windows) showing significantly higher/lower 5mC levels in ESCs compared with EpiLCs and those showing relatively greater sensitivity/resistance to demethylation in d6 PGCLCs (Figure 3A). Such regions often formed clusters: we designated both singlet regions and clusters selected under certain criteria as domains (see Experimental Procedures). We thus identified hypo-/hypermethylated domains in ESCs and demethylation-sensitive/-resistant domains in PGCLCs (Figure 3B). There were 11 domains that were hypermethylated in ESCs but less so in EpiLCs, but these were not studied further because of the lack of associated genes.

Hypomethylated Domains in ESCs

The domains significantly hypomethylated in ESCs compared with EpiLCs (3,309 in total) occupied 2.1% of the genome and showed higher (G + C) content than the total unique regions (Figures 3C and 3D; Table S4). Upon ESC-to-EpiLC transition, the hypomethylated state of the domains became less recognizable with an increase in their 5mC level and, upon PGCLC induction, became even less so with a progressive dilution of the methylome (Figure 3E). Thus, these hypomethylated domains were specifically observed in ESCs.

The hypomethylated domains in ESCs were gene rich (Figure 3C), and 2,929 promoters (1,958 HCPs, 399 ICPs, and 572 LCPs) were located in and around these domains (Figure S3A). A gene ontology (GO) analysis revealed their association with negative/positive regulation of transcription and chromosome organization, and the gene list included key regulators of pluripotency and components of polycomb repressive complexes (PRCs) (Figure 3F). Based on our histone mark data (Kurimoto et al., 2015), these domains were depleted of H3K27 trimethylation (H3K27me3), enriched in H3K27ac, particularly in ESCs (Figure 3G), and associated with the majority of ESC-specific enhancers (972 of 1,193) (Kurimoto et al., 2015) (Figure S3B). Some of these domains coincided with superenhancer domains formed in CTCF-mediated chromatin loops (Dowen et al., 2014) (Figure S3C). Furthermore, the promoters located in and around the domains were frequently marked by H3K4me3, depleted of H3K27me3, and highly active in ESCs (Figures 3H and 3I). Thus, the hypomethylated domains represent active chromatin associated with robust transcription in ESCs.

Demethylation-Sensitive Domains in PGCLCs

The demethylation-sensitive domains in PGCLCs (91 in total) occupied 0.05% of the genome and were (G + C) rich (Figures 3C and 3D; Table S4). These domains showed faster demethylation than the rest of the genome, reaching the minimum 5mC level of 12.5% in d6 PGCLCs (Figure 3E).

The demethylation-sensitive domains in PGCLCs were gene rich (Figure 3C), and 153 promoters (103 HCPs, 40 ICPs, and 10 LCPs) were found in and around the domains (Figure S3A). These genes were often involved in pattern specification or embryonic morphogenesis (Figure 3F). Only 6.5% of these genes overlapped with those identified in and around the hypomethylated domains in ESCs (Figure S3D). To explore this point further, we examined ESCs cultured with 1.0 μM MEKi (Habibi et al., 2013) and found that, although the hypomethylated domains expanded greatly to encompass about half of all genes (Figures S3E and S3F), more than 70% of the genes found in and around the demethylation-sensitive domains in PGCLCs were still excluded (Figure S3F). Thus, the mechanism and targets of demethylation mediated by MEKi in ESCs are distinct from those observed in PGCLC development.

The demethylation-sensitive domains were marked by H3K27me3, devoid of H3K27ac in both d2 and d6 PGCLCs (Figure 3G), and identified previously as "d2 or d6 PGCLC PRC2 targets" (112 of 153) (Kurimoto et al., 2015) (Figure S3G). Consistently, the promoters of the genes identified in and around these domains were marked by H3K27me3, depleted of H3K4me3, and transcriptionally repressed in d6 PGCLCs (Figures 3H and 3I). Thus, the demethylation-sensitive domains in PGCLCs assume repressive chromatin and show no or only low transcriptional activity.

Demethylation-Resistant Domains in PGCLCs

The relatively demethylation-resistant domains in PGCLCs (340 in total) accounted for 0.1% of the genome and showed (G + C) content similar to that of the total unique regions (Figures

The background plots in the bottom panels are from the promoters (middle). A yellow dotted line connects the origin and mode. The regression line for the repeats is colored in magenta. Color coding is as indicated in the lower panel of (A).

(C) Heatmaps showing the 5mC levels of indicated genomic elements in indicated cells. One hundred promoters and enhancers of each class (Kurimoto et al., 2015) and 400 non-promoter CGIs (Illingworth et al., 2010), exons, introns, and intergenic regions (2-kb windows) are randomly selected and analyzed. Color coding is as indicated.

(D and E) Relative changes in 5mC level of indicated elements during PGCLC induction and PGC development (Kobayashi et al., 2013). The 5mC levels determined in EpiLCs are used as reference. Color coding is as indicated.

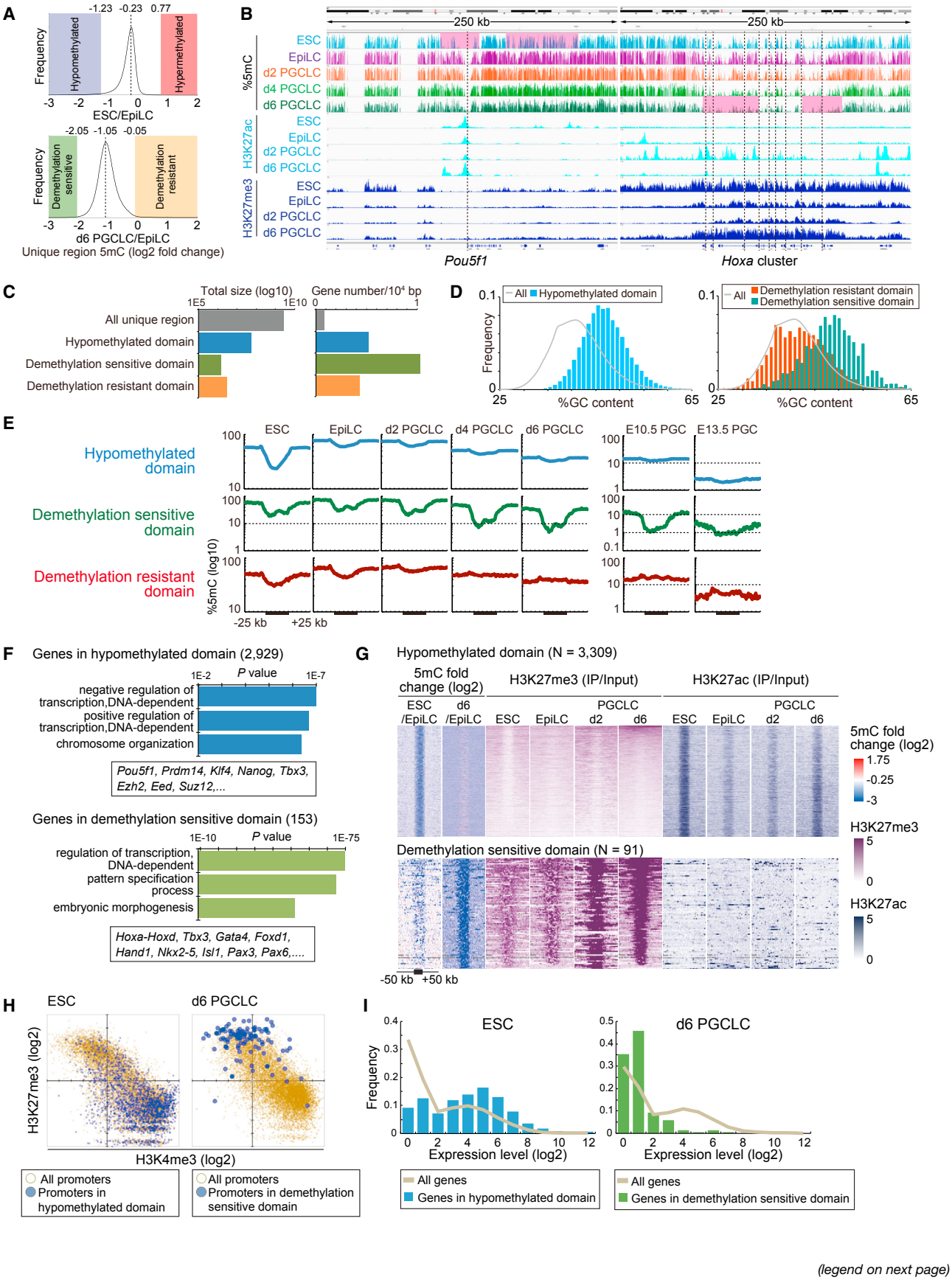

(legend on next page)

3C and 3D; Table S4). They were considerably methylated, but at slightly lower 5mC levels compared with the adjacent regions, in both ESCs and EpiLCs (Figure 3E). These domains had a highest 5mC level in d2 PGCLCs, and showed resistance to demethylation in d4 and d6 PGCLCs, maintaining the relatively high 5mC levels in d6 PGCLCs (Figure 3E). About 20% of the demethylation-resistant domains were located on the Y chromosome (Table S4).

The demethylation-resistant domains were gene rich (Figure 3C) and, based on our previous data (Kurimoto et al., 2015), marked by H3K27ac in d6 PGCLCs (Figure S3H). A total of 136 promoters (64 HCPs, 37 ICPs, and 35 LCPs) were identified in and around the domains (Figure S3A), which overlapped significantly with those identified in and around the hypomethylated domains in ESCs (95 of 136, 70%) (Figure S3D). These genes showed association with cell-cell adhesion or transcription (Figure S3I). The H3K27me3 and H3K4me3 levels and transcriptional activity of the promoters were similar to those of all promoters (Figures S3J and S3K). Thus, despite the demethylation resistance and retention of considerable levels of 5mC, these promoters showed activity in d6 PGCLCs.

Promoter and Enhancer Methylation and Transcription

We next explored the influence of promoter methylation on gene expression. More than 96% of the promoters that showed $\geq$20% methylation in at least one cell type were ICPs and LCPs, and the vast majority of HCPs stayed hypomethylated (<20%) (Figure 4A). Since all cell types predominantly express HCP genes (Kurimoto et al., 2015), the DNA methylation reprogramming appeared to regulate only a small set of genes during PGCLC induction.

We identified promoters showing significant hypomethylation in ESCs compared with EpiLCs (930) (there were none with significant hypermethylation in ESCs) and those showing sensitivity (179) or resistance (258) to demethylation in d6 PGCLCs (Figure 4B). We noted overlaps between the categories: 67 of the 930 hypomethylated-in-ESC promoters were demethylation sensitive and another set of 67 were demethylation resistant in d6 PGCLCs (Table S5). Figures 4C and S4A show the changes in 5mC and expression levels observed with the promoters representative of the three categories. While the hypomethylated-in-ESC promoters were enriched for genes involved in immune response and showed an expected reverse correlation between the 5mC and expression levels, the demethylation-sensitive promoters were enriched for genes involved in embryonic morphogenesis and showed a less significant correlation between the 5mC and expression levels (Figures 4D and 4E). Notably, the demethylation-resistant promoters showed enrichment for genes involved in meiosis, gained methylation in d2 PGCLCs, and showed a reverse correlation between 5mC and expression (Figures 4B, 4D, and 4E). This is consistent with the notion that the germline genes are tightly regulated by DNA methylation (Seisenberger et al., 2012). While 32% of the hypomethylated-in-ESC promoters were located in the hypomethylated domains, only 12% and 10% of the demethylation-sensitive and -resistant promoters, respectively, were located within the corresponding domains in d6 PGCLCs (Figure 4F). Thus, the regulation of DNA methylation at the demethylation-resistant promoters of the meiosis-related genes appears local.

We tried to correlate the 5mC levels of the ESC- and d6-PGCLC-specific enhancers, marked by H3K27ac in the corresponding cell types (Kurimoto et al., 2015), with the expression levels of the nearby genes. While many ESC-specific enhancers showed hypomethylation in ESCs, only a few d6-PGCLC-specific enhancers were sensitive to demethylation in d6 PGCLCs (Figure 4G). Thus, promoter/enhancer hypomethylation, expression, and domain-wide hypomethylation showed a good correlation in ESCs but not in PGCLCs.

Role of PRDM14 in DNA Methylation Reprogramming

We next explored the impact of loss of PRDM14, a key regulator of naive pluripotency and PGC specification (Ma et al., 2011; Yamaji et al., 2008, 2013), on the transcriptome and methylome during PGCLC induction. It was previously shown that ablation of *Prdm14* in mice results in inefficient derivation and survival of ESCs, impaired PGC development, and infertility (Yamaji et al., 2008, 2013). Compared with wild-type cells, *Prdm14*$^{-/-}$ ESCs showed altered expression ($\geq$2-fold) of 504 genes, but only 139 genes were affected in mutant EpiLCs (Figure 5A). The functional significance of PRDM14 became greater again upon PGCLC induction: 415 genes were affected in mutant d6 PGCLCs (Figure 5A). Only a small number of genes showed consistently higher or lower expression in both mutant ESCs

Figure 3. Distinct Correlations between DNA Hypomethylation, Histone Modifications, and Transcription in ESCs and d6 PGCLCs

(A) Histograms showing the distributions of the unique regions (2-kb windows) across 5mC fold changes in ESC and EpiLC (top) and in d6 PGCLC and EpiLC (bottom). The mode values and criteria for hypo-/hypermethylated domains in ESCs and demethylation-sensitive/-resistant domains in PGCLCs are indicated.

(B) Screenshots of the 5mC, H3K27ac, and H3K27me3 distributions in representative regions. Hypomethylated domains in ESCs (*Pou5f1*) and demethylation-sensitive domains in PGCLCs (*Hoxa*) are highlighted in pink. Positions of the transcription start sites are indicated by vertical dotted lines.

(C) Total sizes (left) and gene densities (right) of the unique regions, hypomethylated domains in ESCs, and demethylation-sensitive/-resistant domains in PGCLCs.

(D) Histograms showing the distributions of 2-kb windows from the hypomethylated domains in ESCs (left) and demethylation-sensitive/-resistant domains in PGCLCs (right) across (G + C) content. The distribution of all unique regions is shown for comparison.

(E) Aggregation plots showing the 5mC levels in and around indicated domains in indicated cells. Published data are used for PGCs (Kobayashi et al., 2013).

(F) GO term enrichment and representative genes in and around indicated domains.

(G) Heatmaps showing the 5mC fold changes and H3K27me3 and H3K27ac levels in and around the hypomethylated domains in ESCs and demethylation-sensitive domains in PGCLCs in indicated cells. Color coding is as indicated.

(H) Scatterplots showing the correlations between the H3K4me3 and H3K27me3 levels at the promoters located in and around the hypomethylated domains in ESCs (left) and demethylation-sensitive domains in d6 PGCLCs (right). The correlations at all promoters are shown for comparison.

(I) Histograms showing the distributions of the genes in and around the hypomethylated domains in ESCs (left) and demethylation-sensitive domains in d6 PGCLCs (right) across expression levels. The distribution of all genes is shown for comparison.

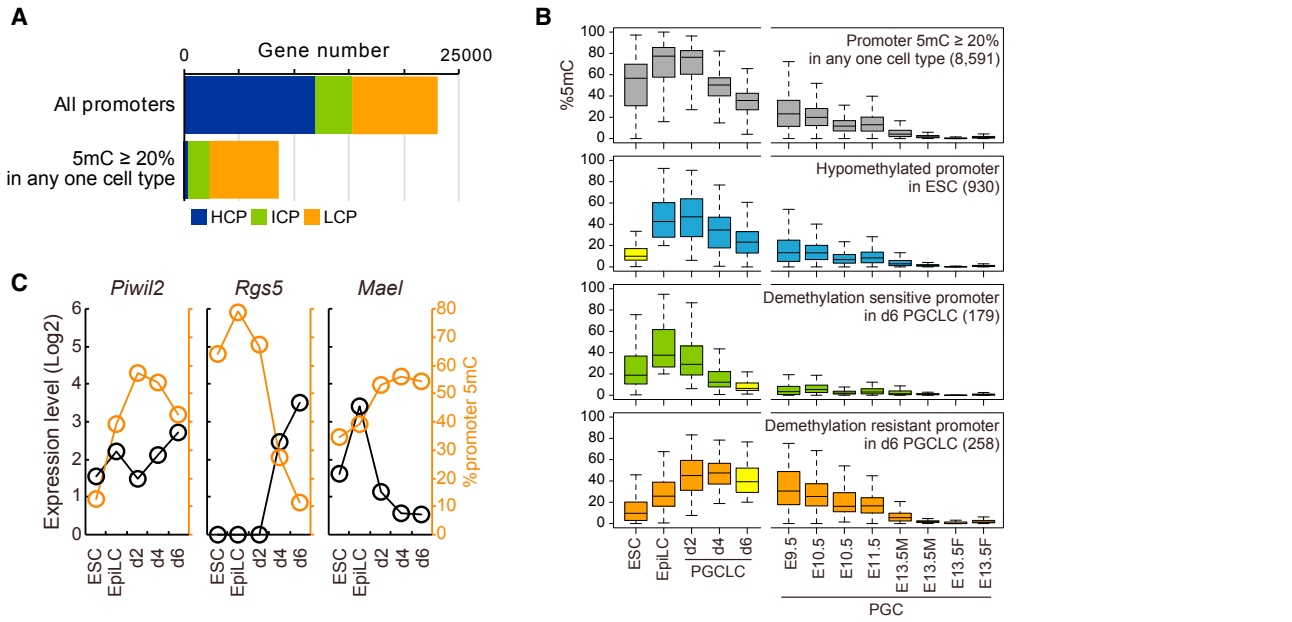

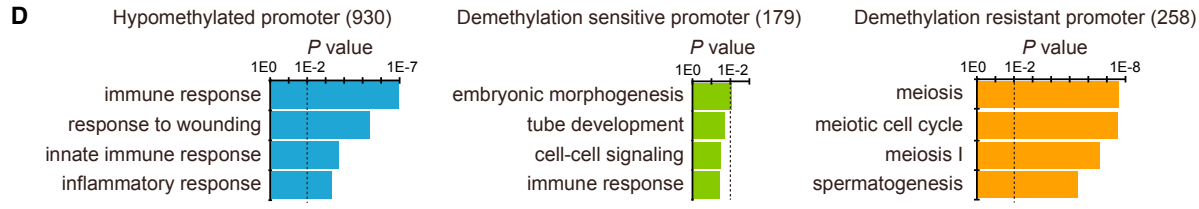

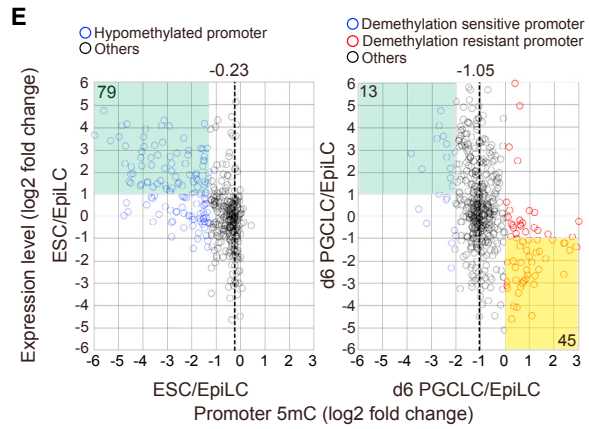

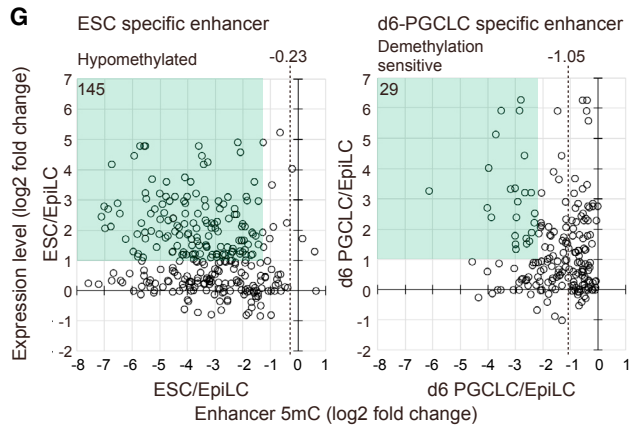

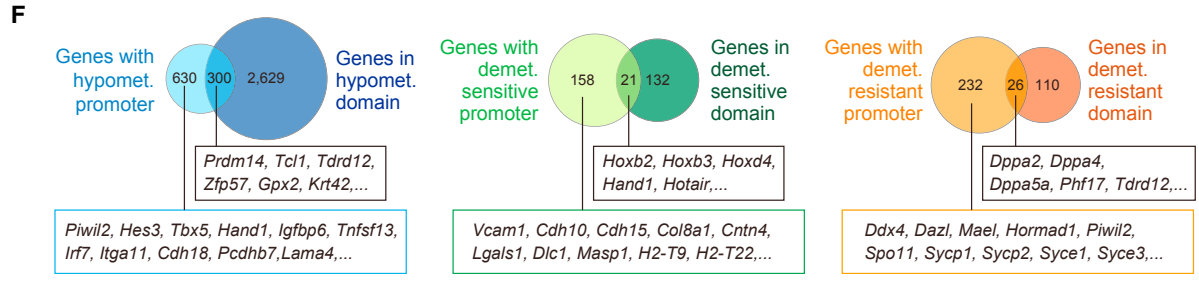

(legend on next page)

and d6 PGCLCs (Figure 5B), suggesting that PRDM14 regulates different sets of genes in ESCs and PGCLCs.

In *Prdm14*$^{-/-}$ PGCLCs, expression of *Tfap2c*, *Nanos3*, and *Sox2*, which are the key genes for PGC specification and potential pluripotency, was delayed (Figure 5C), suggesting that PRDM14 is important for timely induction of these genes. Consistent with the previous report (Yamaji et al., 2013), mutant ESCs derepressed *Dnmt3a*, *Dnmt3b*, and *Dnmt3l* (Figure 5C), supporting the notion that PRDM14 plays an important role in repressing de novo DNA methylation. Importantly, mutant PGCLCs failed to repress *Uhrf1*, a key regulator of maintenance methylation (Bostick et al., 2007; Sharif et al., 2007), and *Dnmt3* (Figure 5C), suggesting that PRDM14 represses these genes for global demethylation. Since the loss of *Prdm14* did not affect *Uhrf1* expression in ESCs (Figure 5C), ESCs and PGCLCs have differential requirements for PRDM14 in the regulation of maintenance methylation activity.

Consistent with the previous work on limited loci (Yamaji et al., 2013) and also with the expression profile described above, *Prdm14*$^{-/-}$ ESCs and EpiLCs showed higher global 5mC levels (76% and 82%, respectively) compared with wild-type cells (58% and 73%, respectively) (Figures 5D and S5A; Table S1). Mutant cells also showed higher 5mC levels in the promoters, particularly in the ICPs and LCPs (Figure 5D). Upon PGCLC induction, mutant cells underwent progressive, but slower and lesser demethylation. Thus, the global 5mC level was 68% in mutant d6 PGCLCs compared with 37% in wild-type cells (Figures 5D and S5A; Table S1). Since mutant PGCLCs showed a cell-cycle profile similar to that of wild-type cells (Figures S5B and S5C), the slower demethylation was not due to less frequent DNA replication. Scatterplot comparisons of the 5mC levels between mutant EpiLCs and d6 PGCLCs revealed uneven demethylation (Figure 5E), suggesting the existence of regions more/less sensitive to the mutation. Indeed, the HCPs, ICPs, non-promoter CGIs, and EpiLC- and PGCLC-specific enhancers were less sensitive to the mutation than the other elements (Figure 5F). In contrast, the repeats and ICRs were clearly sensitive and showed higher 5mC levels in mutant PGCLCs (Figures 5E and S5D), indicating that these elements require PRDM14 for demethylation in PGCLCs.

There were 3-fold fewer hypomethylated domains, with a smaller average size, in *Prdm14*$^{-/-}$ ESCs compared with wild-type cells (Figure S5E and Table S4). With an exception of genes associated with stem cell maintenance, many genes located in and around the hypomethylated domains in wild-type ESCs were no more associated with such domains in mutant cells (Figure 5G). In contrast, the number and size of demethylation-sensitive domains were comparable between mutant and wild-type d6 PGCLCs (Figure S5E and Table S4). Thus, the same developmental genes marked by H3K27me3 (see above) were found in the demethylation-sensitive domains in both wild-type and mutant PGCLCs (Figure 5G).

DNA Methylation Reprogramming during Female PGCLC Specification

Female ESCs have two active X chromosomes (Xa) and show extremely lower global 5mC levels than male ESCs (Habibi et al., 2013; Schulz et al., 2014; Zvetkova et al., 2005). Also, a majority of female EpiLCs maintain the XaXa pattern and, upon differentiation, undergo X chromosome inactivation. Female PGCLCs initially have one Xa and one inactive X chromosome (Xi) and gradually reactivate the Xi (Hayashi et al., 2012).

We first examined the methylomes of female ESCs, EpiLCs, and d6 PGCLCs, and found that not only ESCs but also other cell types have lower 5mC levels in the unique regions and promoters in females compared with males (Figures 6A and 6B). We then examined the transcriptomes of these cells. Female ESCs, EpiLCs, and d6 PGCLCs respectively express 341, 321, and 322 genes at higher levels ($\geq$2-fold) and 464, 105, and 208 genes at lower levels ($\leq$0.5-fold), compared with male counterparts (Figure 6C). Thus, the global hypomethylation affects gene expression in either direction. Only a small subset of genes consistently showed higher or lower expression in all female cells (Figure 6D). Consistent with the XaXa state, expression of X-linked genes was 1.9-fold higher in female ESCs and EpiLCs, and 1.5-fold higher in female d6 PGCLCs compared with male counterparts (Figure S6A). The key genes for PGC specification and DNA methylation/demethylation were expressed similarly in males and females during PGCLC development, except for *Tcl1* and *Dnmt3l*, which showed higher expression in female cells (Figure 6E).

Upon ESC-to-EpiLC transition, female cells drastically increased the global 5mC level (from 21% to 64%), acquiring a reorganized methylome similar to that of male cells (Figures 6A, 6F, and S6B; Table S1). Female PGCLCs then rapidly lost methylation (0.5-fold per 2 days) and reached the global 5mC level of 16% in d6 PGCLCs (Figures 6A, 6F, and S6B; Table S1), acquiring essentially a diluted version of the EpiLC

Figure 4. Promoter and Enhancer Methylation and Transcription

(A) Proportions of HCP, ICP, and LCP in all promoters and in those showing 5mC level $\geq$20% in at least one cell type.

(B) Box-and-whisker plots of the 5mC levels of indicated promoters during PGCLC induction and PGC development (Kobayashi et al., 2013; Seisenberger et al., 2012). M, male; F, female.

(C) Changes in promoter 5mC level (orange) and expression level (black) of *Piwil2* (a promoter hypomethylated in ESCs and demethylation-resistant in d6 PGCLCs), *Rgs5* (demethylation-sensitive), and *Mael* (demethylation-resistant) during PGCLC induction.

(D) GO term enrichment for indicated promoters.

(E) Scatterplots showing the correlations between the fold changes in 5mC and expression in ESCs and EpiLCs (left) and in d6 PGCLCs and EpiLCs (right) for indicated promoter categories. Dotted lines indicate the mode values of the 5mC fold changes in all unique regions (Figure 3A). The numbers of genes showing positive and negative correlations are indicated.

(F) Venn diagrams showing the overlaps between the genes identified by 5mC change in domains and those identified by 5mC change in promoters. Demet., demethylation; hypomet., hypomethylation.

(G) Scatterplots showing the correlations between the fold changes in 5mC and expression in ESCs and EpiLCs (left) and in d6 PGCLCs and EpiLCs (right) for indicated enhancer categories. Dotted lines indicate the mode values of the 5mC fold changes in all unique regions (Figure 3A). The numbers of genes showing expected positive correlations are indicated.

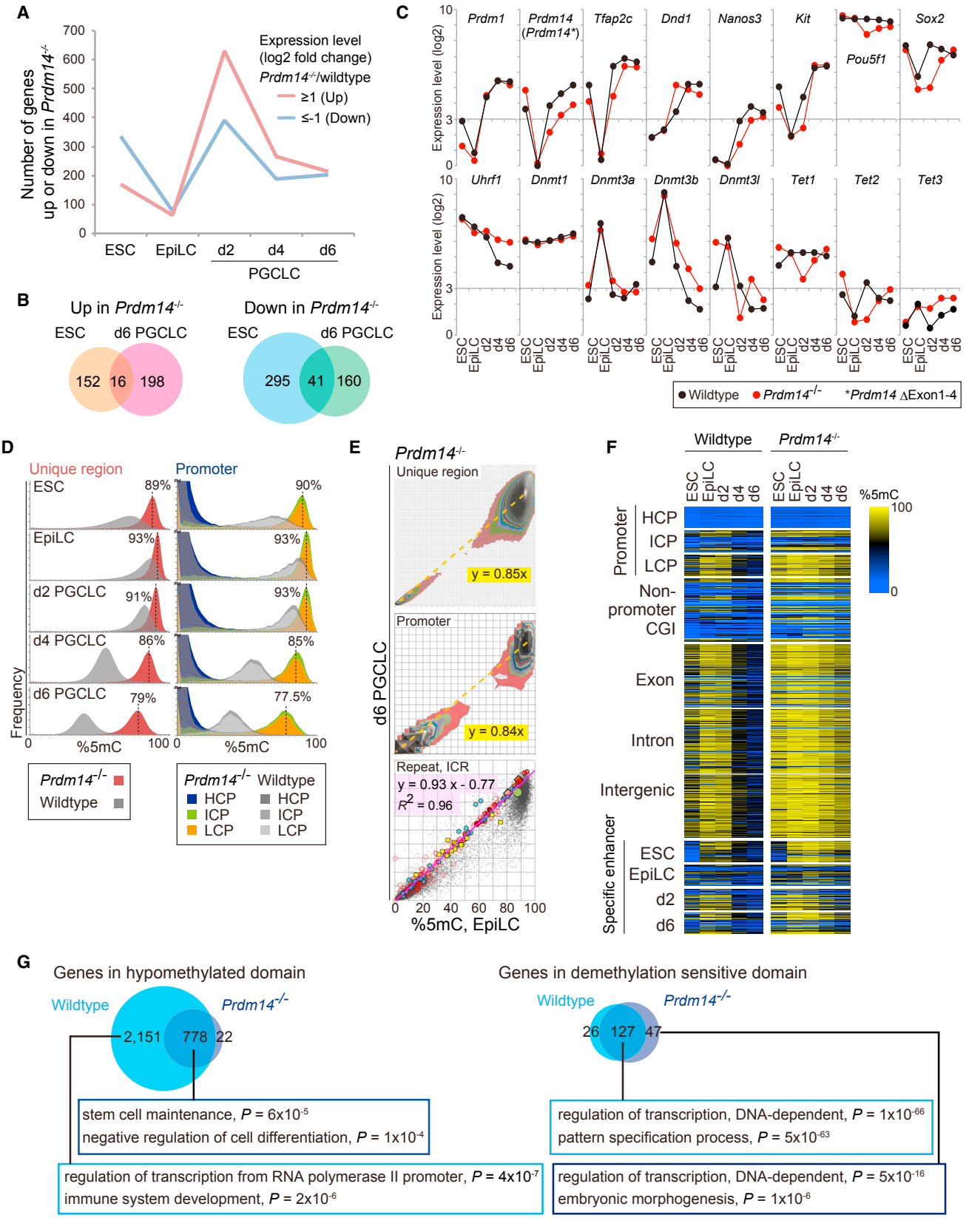

(legend on next page)

methylome (Figure 6F). Thus, female cells essentially follow the changes observed in male cells. However, severe loss of 5mC occurred in almost all ICRs in female cells: the DNA methylation imprints were lost in ESCs, not re-established in EpiLCs except for the *Rasgrf1* and *H19* ICRs, and erased further in d6 PGCLCs (Figures 6F, S6C, and S6D). In contrast, the 5mC levels of many repeats, including IAPs and satellites, were better preserved (Figure 6F). Thus, upon PGCLC induction, female cells undergo DNA methylation reprogramming under the principle similar to that of male cells, with more acute global changes and distinct impacts on specific elements.

We identified hypomethylated domains in female ESCs and demethylation-sensitive/-resistant domains in female PGCLCs (Figure S6E and Table S4). There were 4-fold more hypomethylated domains in female ESCs compared with male cells, with twice the average size of those in male cells (see next section). A large number of genes existed in and around the hypomethylated domains of female ESCs, including those found in such domains of male cells (Figure 6G). Although there were more, and larger, demethylation-resistant domains in female d6 PGCLCs compared with male cells, the demethylation-sensitive domains showed modest differences between male and female cells (Figures 6G and S6E; Table S4).

Hypomethylated Mega-Domains in Female ESCs

When we compared the 5mC levels of the unique regions between male and female ESCs in 500-kb windows, two distinct populations of genomic domains were noted. One population showed a relatively even and proportional decrease in 5mC level in female ESCs compared with male cells, while the other showed greater and uneven decreases in female cells (Figure 7A). The two populations were also distinguishable in ESCs cultured with serum or with 1 μM MEKi (Habibi et al., 2013) (Figure S7A). The domains of the latter population often existed next to each other and formed mega-domains as large as 12.5 Mb (average 1.9 Mb) (Figure S7B and Table S4). These mega-domains showed lower 5mC levels compared with the adjacent regions in female ESCs and EpiLCs, but not in their male counterparts, or in d6 PGCLCs and E13.5 PGCs of either sex (Figure 7B). Thus, female PGCLCs effectively reverse the hypomethylated states of such domains into a more normal configuration.

The hypomethylated mega-domains in female ESCs showed low (G + C) content and low gene density (Figures 7C and 7D) and overlapped significantly with constitutive lamina-associated domains (cLADs), which are marked by H3K9me2 (Guelen et al., 2008; Peric-Hupkes et al., 2010) (Figures 7E and S7B). The promoters located in the hypomethylated mega-domains were predominantly LCPs (Figure S7C) and stayed silenced in both male and female ESCs, EpiLCs, and PGCLCs (Figure 7F). We recently reported large partially methylated domains in prospermatogonia (PSGs) and more differentiated spermatogenic cells (Kubo et al., 2015), which essentially overlap with the cLADs. As expected, the hypomethylated mega-domains overlapped well with the partially methylated domains identified in E16.5 PSGs and adult spermatozoa (Kobayashi et al., 2013; Kubo et al., 2015) (Figure S7B). Although less prominent, the hypomethylated mega-domains were also present in germinal-vesicle oocytes (Shirane et al., 2013) (Figure 7B). The methylome of female ESCs correlated relatively well with that of E16.5 PSGs, but less so with those of sperm and germinal-vesicle oocytes, which have the established methylomes (Figure S7D). These findings suggest unique methylome regulation in female ESCs, the mechanism of which might operate during the de novo methylation process in germ cell development.

DISCUSSION

The present study uncovers the dynamic DNA methylation reprogramming at the outset of mouse germ cell development in the in vitro PGCLC induction system and, combined with our previous work (Kurimoto et al., 2015), illuminates the unique orchestration of DNA methylation and histone modification reprogramming. As summarized in Figure 7G, ESCs reorganize their methylome, especially around pluripotency regulators, by de novo DNA methylation and H3K27ac removal, to form EpiLCs. Then the PGCLCs essentially dilute the EpiLC methylome and deposit H3K27me3 around developmental regulators for their repression. PRDM14 plays an important role in these processes, especially in maintaining the hypomethylated state of pluripotency regulators in ESCs and establishing the global hypomethylation state in PGCLCs. Although female cells generally show lower methylation levels compared with male cells, the regulatory principle for DNA methylation reprogramming is essentially the same in both sexes. Interestingly, hypomethylated mega-domains exist in female ESCs and EpiLCs, overlapping with the cLADs marked by H3K9me2, but disappear upon PGCLC differentiation to form a more normal methylome (Figure 7G).

Our data suggest that the global DNA demethylation during PGCLC specification proceeds primarily via a replication-coupled passive mechanism through repression of DNA

Figure 5. Role of PRDM14 in DNA Methylation Reprogramming

(A) Numbers of genes showing higher (red) and lower expression (blue) in *Prdm14*$^{-/-}$ cells compared with wild-type cells.

(B) Venn diagrams showing the overlaps between the genes showing higher expression in *Prdm14*$^{-/-}$ ESCs and in d6 PGCLCs (left) and between the genes showing lower expression in the two cell types (right).

(C) Expression levels ($\log_2$[FPKM + 1]) of key genes in *Prdm14*$^{-/-}$ (red) and wild-type cells (black) during PGCLC induction. An asterisk indicates the transcripts from the mutated *Prdm14* allele (exons 1–4 deleted).

(D) Histograms showing the distributions of the unique regions (2-kb windows) (left) and promoters (right) across 5mC levels in indicated *Prdm14*$^{-/-}$ cells. The mode 5mC levels are indicated for the unique regions and LCPs. Histograms from wild-type cells (Figure 2A) are shown for comparison. Color coding is as indicated.

(E) Comparisons of the 5mC levels of indicated genomic elements between indicated *Prdm14*$^{-/-}$ cells. Details are as for Figure 2B.

(F) Heatmaps showing the 5mC levels of indicated genomic elements in indicated *Prdm14*$^{-/-}$ cells. Heatmaps from wild-type cells (Figure 2C) are shown for comparison. Details are as for Figure 2C.

(G) Venn diagrams showing the overlaps between the genes identified in *Prdm14*$^{-/-}$ and wild-type cells. The genes identified in and around the hypomethylated domains in ESCs (left) and demethylation-sensitive domains in PGCLCs (right) are separately shown. GO term enrichment is shown for indicated genes.

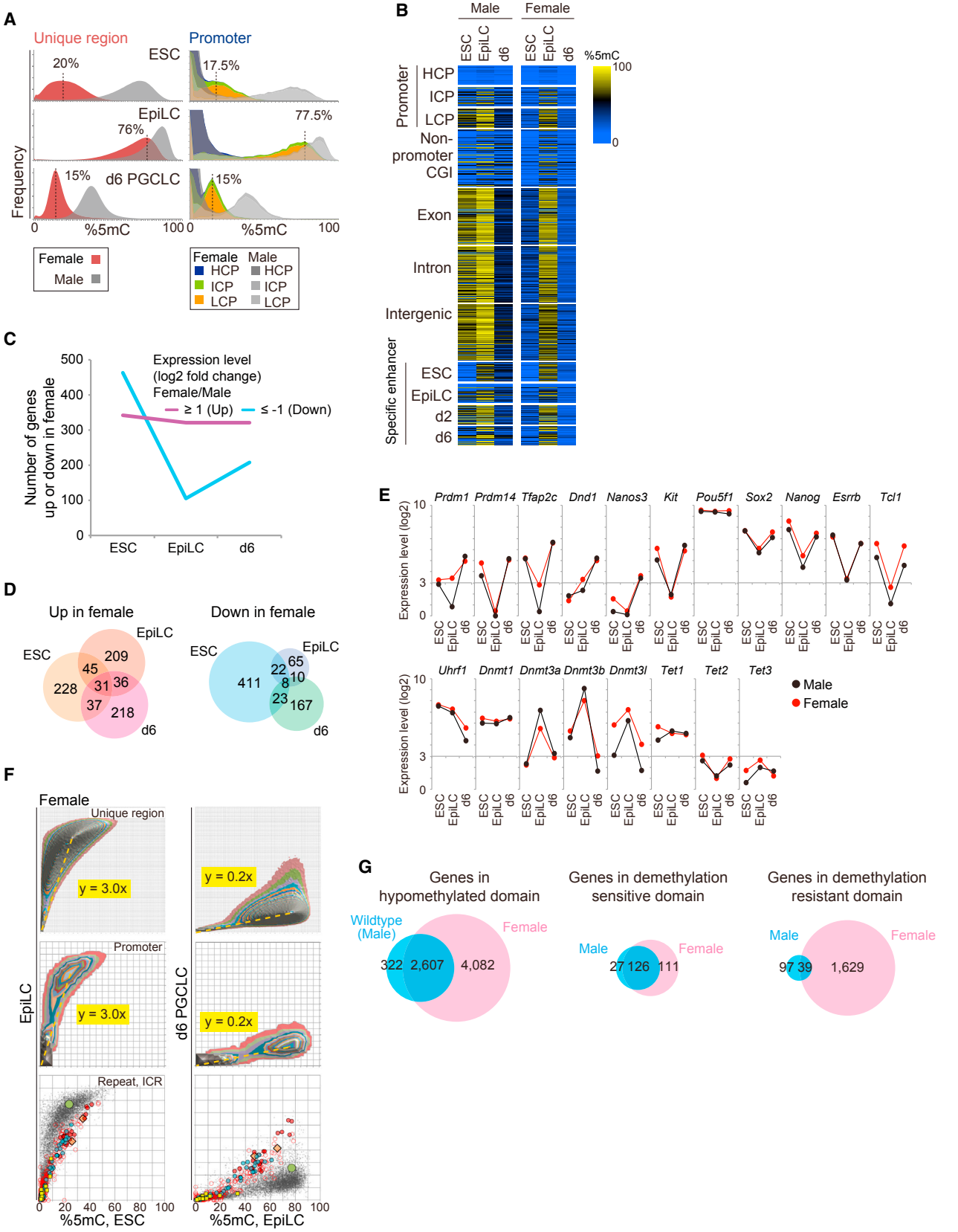

(legend on next page)

methyltransferase (DNMT) activity (Figures 1, 2, and 5), as reported for more developed PGCs (E9.5 and later) (Arand et al., 2015; Kagiwada et al., 2013; Seisenberger et al., 2012). Consistent with this notion, mutant PGCLCs, deficient in proper repression of *Uhrf1* and *Dnmt3b*, fail to erase the EpiLC methylome (Figure 5). Together with the data showing the lack of both TET activation and 5hmC accumulation (Figures 1 and 5), our study discounts the other possible mechanism involving global 5hmC accumulation followed by dilution or active demethylation. In this regard, it is interesting that the global demethylation in ESCs cultured in 2i also occurs by a passive mechanism, involving a reduction in UHRF1 protein, but not mRNA, and global loss of H3K9me2, which is required for chromatin binding of UHRF1 (von Meyenn et al., 2016).

Interestingly, while the rate of this demethylation is 0.7-fold per 2 days in wild-type male PGCLCs (Figure 2), the cells proliferate 2-fold per 2 days (Hayashi et al., 2011). Thus, there should be a mechanism that withstands the replication-coupled halving of the 5mC level. Notably, the repeat elements generally show greater resistance against the 5mC dilution than the rest of the genome (0.86-fold per 2 days) (Figure 2). We assume that residual DNMT activity in PGCLCs would preferentially target the repeats. Interestingly, female PGCLCs show a faster demethylation rate, consistent with the replication-coupled halving (0.5-fold per 2 days) (Figure 6). Since female and male PGCLCs repress *Uhrf1* and *Dnmts* to similar extents (Figure 6), female cells may lack a mechanism for stabilizing the residual DNMT activity or for recruiting such activity to replication foci, possibly due to the upregulation of X-linked genes (Figure S6).

A previous study suggested similarities between ESCs cultured in 2i and in vivo PGCs regarding the methylome and demethylation mechanism (Ficz et al., 2013). Although both ESCs cultured in 2i and PGCLCs appear to employ a passive mechanism for global demethylation (see above), we note differential regulation of *Uhrf1* by PRDM14 between ESCs and PGCLCs (Figure 5). Moreover, we find that ESCs, but not PGCLCs, maintain pluripotency regulators in a discretely hypomethylated state (Figure 3), while PGCLCs rapidly accumulate high levels of H3K27me3 in developmental regulators for their repression (Kurimoto et al., 2015). The H3K27me3 deposition is well correlated with the rapid loss of 5mC from the demethylation-sensitive domains, which could be brought about by tight exclusion of residual DNMT activity by PRCs (Deaton and Bird, 2011). In this regard, it is notable that loss of PRDM14 leads to drastic shrinkage and even disappearance of the hypomethylated domains in ESCs but not the demethylation-sensitive domains in PGCLCs (Figure 5). Similarly, while female ESCs have larger hypomethylated domains compared with male cells, female PGCLCs do not show changes in the demethylation-sensitive domains (Figure 6). Altogether, we find some fundamental differences between ESCs and PGCLCs regarding the methylome regulation.

We also uncover the existence of hypomethylated mega-domains in female ESCs, which broadly overlap the cLADs (Figure 7). Although the average 5mC level is higher, the hypomethylated mega-domains consistently exist as 5mC valleys in EpiLCs, E16.5 PSGs, sperm, and germinal-vesicle oocytes (Figure 7). It would be interesting to explore whether the hypomethylated mega-domains also exist in the ICM and early epiblast of female embryos (Okamoto et al., 2004). The hypomethylated mega-domains observed in female ESCs overlap very well with the partially methylated domains that we recently reported in male germ cells (Kubo et al., 2015). Notably, partially methylated domains, which primarily overlap the cLADs, also exist in cultured cells and cancers, but not in their normal in vivo counterparts (Berman et al., 2012; Hansen et al., 2011; Hon et al., 2012; Lister et al., 2009, 2011; Raddatz et al., 2012). Cells that have hypomethylated mega-domains or partially methylated domains might have similar nuclear architecture, DNMT regulation, or both, but the underlying mechanism and functional significance warrant further investigation.

In summary, our study highlights the unique regulation of the DNA methylation reprogramming during PGCLC specification and, together with our previous report on histone modification reprogramming (Kurimoto et al., 2015), provides an important resource for further mechanistic studies. Reconstitution of germ cell development beyond d6 PGCLCs will be critical for the study of many fundamental questions regarding, for example, the mechanisms of upregulation of germline genes, further maturation of the PGC epigenome, and initiation of spermatogenic and oogenic differentiation.

EXPERIMENTAL PROCEDURES

All animal experiments were performed under the ethical guidelines of Kyoto University and Kyushu University. The experimental procedures for MS, cell-cycle analyses of PGCLCs, analysis of ICRs and repeat elements, and definition of hypo-/hypermethylated domains/promoters in ESCs and demethylation-sensitive/-resistant domains/promoters in d6 PGCLCs are available in Supplemental Experimental Procedures.

Induction and Isolation of PGCLCs

ESCs were cultured in a medium containing 2iLIF (3 μM GSKi [CHIR99021], 0.4 μM MEKi [PD0325901], and 1 U/μL LIF) and induced into EpiLCs, from

Figure 6. DNA Methylation Reprogramming during Female PGCLC Induction

(A) Histograms showing the distributions of the unique regions (2-kb windows) (left) and promoters (right) across 5mC levels in indicated female cells. The mode 5mC level is indicated for the unique regions and LCPs. Histograms from male cells (Figure 2A) are shown for comparison. Color coding is as indicated.

(B) Heatmaps showing the 5mC levels of indicated genomic elements in indicated female cells. Heatmaps from male cells (Figure 2C) are shown for comparison. Details are as for Figure 2C.

(C) Numbers of genes showing higher (red) and lower (blue) expression in female cells compared with male cells.

(D) Venn diagrams showing the overlaps between the genes showing higher (left) or lower (right) expression in female ESCs, EpiLCs, and d6 PGCLCs compared with corresponding male cells.

(E) Expression levels ($\log_2$[FPKM + 1]) of key genes in female (red) and male (black) cells during PGCLC induction.

(F) Comparisons of the 5mC levels of indicated genomic elements between indicated female cells. Details are as for Figure 2B.

(G) Venn diagrams showing the overlaps between the genes identified in male and female cells. The genes identified in and around the respective domains are separately shown.

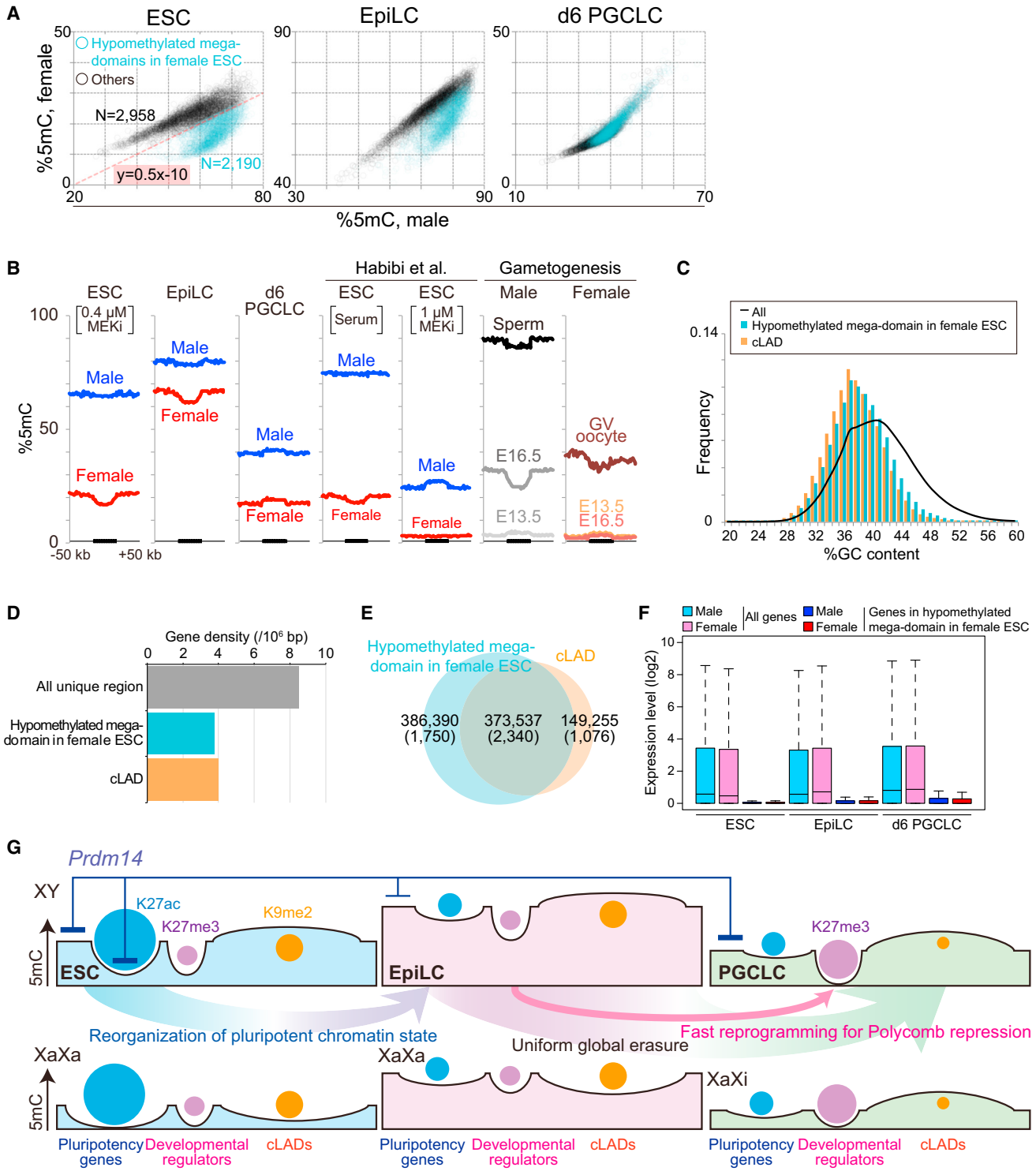

Figure 7. Hypomethylated Mega-Domains in Female ESCs

(A) Scatterplots showing the 5mC levels of the unique regions (500-kb windows) between indicated male and female cells. The hypomethylated mega-domains in female ESCs (blue dots) are defined as domains in $y < 0.5x - 10$, where x and y denote the 5mC levels in male and female ESCs, respectively.

(B) Aggregation plots showing the 5mC levels in and around the hypomethylated mega-domains in indicated male and female cells. Published data are used for ESCs cultured with serum and with 1 μM MEKi (Habibi et al., 2013), PGCs (Kobayashi et al., 2013), sperm (Kubo et al., 2015), and germinal-vesicle oocytes (Shirane et al., 2013).

(C) Histograms showing the (G + C) content of the hypomethylated mega-domains (2-kb windows), cLADs (Guelen et al., 2008; Peric-Hupkes et al., 2010), and all unique regions.

(legend continued on next page)

which PGCLCs were induced as described previously (Hayashi et al., 2011). PGCLCs were purified with a fluorescence-activated cell sorter using the *Blimp1-mVenus* reporter as described previously (Hayashi et al., 2011).

WGBS

Genomic DNA of 50–200 ng spiked with 0.5%–1.0% (w/w) unmethylated lambda phage DNA (Promega) was subjected to bisulfite conversion and library construction for amplification-free WGBS, using the post-bisulfite adaptor tagging method as described previously (Kobayashi et al., 2013; Miura et al., 2012; Shirane et al., 2013). Massively parallel sequencing was performed on an Illumina HiSeq 1500/2500 to generate 101-nt single-end or paired-end sequence reads. Cluster generation and sequencing were performed in single-read/paired-end mode using the TruSeq SR/PE Cluster Kit v3-cBot-HS and the TruSeq SBS Kit v3-HS (Illumina) according to the manufacturer's protocols.

Processing, Mapping, and Conversion of the Data for WGBS

For quality control of the data, we trimmed away 4 and 15 bases from the 5′ ends for single- and paired-end reads, respectively, one base at the 3′ ends, low-quality bases from the 3′ ends (quality score <20), and the adaptor sequences of the libraries, by using the TrimGalore program (http://www.bioinformatics.babraham.ac.uk/projects/trim_galore/). We mapped the processed reads to the mouse reference genome (mm10/GRCM38) using the Bismark program with the options of "-X 1000 –pbat -un" for paired-end reads and "–pbat" for single-end reads (Krueger and Andrews, 2011), and only uniquely mapped reads were used for subsequent analyses. For the paired-end data, we remapped unmapped reads as single-end for read1 with "–pbat" and read2 with default options, and the mapped reads from the single- and paired-end data were combined. The numbers of converted/unconverted CpGs in both strands were combined to determine 5mC levels. To estimate the bisulfite conversion rate, we mapped the processed reads to the lambda phage genome. The sequencing and mapping statistics are shown in Table S1. CpG sites covered by less than five reads and more than 200 reads were excluded; thus the minimum sequence depth to call 5mC level was 5.

Analysis of DNA Methylation in Unique Regions and Promoters

For the unique regions, 5mC levels were determined in 2-kb sliding windows with 1-kb overlaps. Promoters were defined as regions from 0.9 kb upstream to 0.4 kb downstream of the transcription start sites and classified into HCPs, ICPs, and LCPs depending on their (G + C) content and CpG density as described previously (Weber et al., 2007). Promoters with at least five CpG sites were used for methylation analysis. To determine fold changes in 5mC levels between different cell types, we used only unique regions (2-kb windows) and promoters fulfilling the following criteria: (1) 5mC level >20% for either cell type and (2) >0% for both cell types. This effectively excluded contributions by unique regions and promoters showing large fold changes in a low-5mC level range ($\leq$20%).

RNA-Seq

Total RNA of 75–100 ng was used for library construction for RNA-seq analysis. Libraries were prepared using a TruSeq Stranded mRNA Sample Prep Kit (Illumina) according to the manufacturer's instructions, and sequenced on HiSeq1500/2500 to generate 101-nt paired-end sequence reads as described above. After trimming of Illumina adaptor sequences and low-quality bases from the 3′ end (quality score <20) by TrimGalore, the read tags were aligned to mouse RefSeq transcripts by TopHat with the following options: "-g 1 –no-mixed –no-discordant –library-type fr-firststrand." Reads uniquely mapped to gene exons were normalized by total mapped reads and exon lengths (fragments per kilobase of exon per million mapped sequence reads [FPKM]) by the Cufflinks program (Trapnell et al., 2009). The biological replicates of RNA-seq showed good reproducibility (the correlation coefficients were 0.99 for ESCs, EpiLCs, and d6 PGCLCs). We defined genes differentially expressed between two cell types as follows: (1) $\log_2$(FPKM + 1) > 3 in at least one cell type, and (2) difference in $\log_2$(FPKM + 1) $\geq$ 1 (2-fold). The read depth corresponding to $\log_2$ (FPKM + 1) = 3 was in the range of 408–19,551 reads. The sequencing and mapping statistics are shown in Table S2.

See also Supplemental Experimental Procedures.

ACCESSION NUMBERS

The WGBS and RNA-seq data were deposited in the DDBJ/GenBank/EMBL database: DRA003471.

SUPPLEMENTAL INFORMATION

Supplemental Information includes Supplemental Experimental Procedures, seven figures, and five tables and can be found with this article online at http://dx.doi.org/10.1016/j.devcel.2016.08.008.

AUTHOR CONTRIBUTIONS

K.S. and K.K. conducted the overall experiments and analyzed the data with help from Y.Y. M.Y. contributed to the generation of *Prdm14*$^{-/-}$ ESCs. J.S. and S.I. contributed to the MS experiments. A.W. contributed to the massively parallel sequencing. K.H. contributed to the female PGCLC induction. K.S., K.K., M.S., and H.S. conceived the project, designed the experiments, and wrote the manuscript.

ACKNOWLEDGMENTS

We thank M. Miyake, T. Akinaga, J. Oishi (Sasaki laboratory), R. Kabata, N. Konishi, and Y. Sakaguchi (Saitou laboratory) for their assistance. We used the supercomputer of ACCMS at Kyoto University. We are grateful to A. Oka and M. Hagiwara for help with the mass spectrometry. K.S. is a JSPS Research Fellow. The work was supported in part by MEXT grants to H.S. (25112010) and K.K. (24681039, 25650065), by an AMED-CREST grant to H.S., and by a JST-ERATO grant to M.S.

Received: October 21, 2015
Revised: June 29, 2016
Accepted: August 19, 2016
Published: September 15, 2016

REFERENCES

Aramaki, S., Hayashi, K., Kurimoto, K., Ohta, H., Yabuta, Y., Iwanari, H., Mochizuki, Y., Hamakubo, T., Kato, Y., Shirahige, K., et al. (2013). A mesodermal factor, T, specifies mouse germ cell fate by directly activating germline determinants. Dev. Cell *27*, 516–529.

Arand, J., Wossidlo, M., Lepikhov, K., Peat, J.R., Reik, W., and Walter, J. (2015). Selective impairment of methylation maintenance is the major cause of DNA methylation reprogramming in the early embryo. Epigenetics Chromatin *8*, 1.

Berman, B.P., Weisenberger, D.J., Aman, J.F., Hinoue, T., Ramjan, Z., Liu, Y., Noushmehr, H., Lange, C.P., van Dijk, C.M., Tollenaar, R.A., et al. (2012). Regions of focal DNA hypermethylation and long-range hypomethylation in colorectal cancer coincide with nuclear lamina-associated domains. Nat. Genet. *44*, 40–46.

(D) Gene densities in the unique regions, hypomethylated mega-domains, and cLADs.
(E) Venn diagram showing the overlap between the hypomethylated mega-domains and cLADs. The numbers indicate the overlap in kilobases with gene number in parentheses.
(F) Box-and-whisker plots showing the expression levels of the genes in the hypomethylated mega-domains and all genes in indicated male and female cells. Color coding is as indicated.
(G) Model of the regulatory logic for the DNA methylation and histone modification reprogramming during in vitro PGC specification.

Bostick, M., Kim, J.K., Esteve, P.O., Clark, A., Pradhan, S., and Jacobsen, S.E. (2007). UHRF1 plays a role in maintaining DNA methylation in mammalian cells. Science *317*, 1760–1764.

Deaton, A.M., and Bird, A. (2011). CpG islands and the regulation of transcription. Genes Dev. *25*, 1010–1022.

Dowen, J.M., Fan, Z.P., Hnisz, D., Ren, G., Abraham, B.J., Zhang, L.N., Weintraub, A.S., Schuijers, J., Lee, T.I., Zhao, K., et al. (2014). Control of cell identity genes occurs in insulated neighborhoods in mammalian chromosomes. Cell *159*, 374–387.

Ficz, G., Hore, T.A., Santos, F., Lee, H.J., Dean, W., Arand, J., Krueger, F., Oxley, D., Paul, Y.L., Walter, J., et al. (2013). FGF signaling inhibition in ESCs drives rapid genome-wide demethylation to the epigenetic ground state of pluripotency. Cell Stem Cell *13*, 351–359.

Gkountela, S., Zhang, K.X., Shafiq, T.A., Liao, W.W., Hargan-Calvopina, J., Chen, P.Y., and Clark, A.T. (2015). DNA demethylation dynamics in the human prenatal germline. Cell *161*, 1425–1436.

Guelen, L., Pagie, L., Brasset, E., Meuleman, W., Faza, M.B., Talhout, W., Eussen, B.H., de Klein, A., Wessels, L., de Laat, W., et al. (2008). Domain organization of human chromosomes revealed by mapping of nuclear lamina interactions. Nature *453*, 948–951.

Guo, F., Yan, L., Guo, H., Li, L., Hu, B., Zhao, Y., Yong, J., Hu, Y., Wang, X., Wei, Y., et al. (2015). The transcriptome and DNA methylome landscapes of human primordial germ cells. Cell *161*, 1437–1452.

Habibi, E., Brinkman, A.B., Arand, J., Kroeze, L.I., Kerstens, H.H., Matarese, F., Lepikhov, K., Gut, M., Brun-Heath, I., Hubner, N.C., et al. (2013). Whole-genome bisulfite sequencing of two distinct interconvertible DNA methylomes of mouse embryonic stem cells. Cell Stem Cell *13*, 360–369.

Hackett, J.A., Sengupta, R., Zylicz, J.J., Murakami, K., Lee, C., Down, T.A., and Surani, M.A. (2013). Germline DNA demethylation dynamics and imprint erasure through 5-hydroxymethylcytosine. Science *339*, 448–452.

Hansen, K.D., Timp, W., Bravo, H.C., Sabunciyan, S., Langmead, B., McDonald, O.G., Wen, B., Wu, H., Liu, Y., Diep, D., et al. (2011). Increased methylation variation in epigenetic domains across cancer types. Nat. Genet. *43*, 768–775.

Hayashi, K., Ohta, H., Kurimoto, K., Aramaki, S., and Saitou, M. (2011). Reconstitution of the mouse germ cell specification pathway in culture by pluripotent stem cells. Cell *146*, 519–532.

Hayashi, K., Ogushi, S., Kurimoto, K., Shimamoto, S., Ohta, H., and Saitou, M. (2012). Offspring from oocytes derived from in vitro primordial germ cell-like cells in mice. Science *338*, 971–975.

Hayatsu, H., and Shiragami, M. (1979). Reaction of bisulfite with the 5-hydroxymethyl group in pyrimidines and in phage DNAs. Biochemistry *18*, 632–637.

Hon, G.C., Hawkins, R.D., Caballero, O.L., Lo, C., Lister, R., Pelizzola, M., Valsesia, A., Ye, Z., Kuan, S., Edsall, L.E., et al. (2012). Global DNA hypomethylation coupled to repressive chromatin domain formation and gene silencing in breast cancer. Genome Res. *22*, 246–258.

Illingworth, R.S., Gruenewald-Schneider, U., Webb, S., Kerr, A.R., James, K.D., Turner, D.J., Smith, C., Harrison, D.J., Andrews, R., and Bird, A.P. (2010). Orphan CpG islands identify numerous conserved promoters in the mammalian genome. PLoS Genet. *6*, e1001134.

Irie, N., Weinberger, L., Tang, W.W., Kobayashi, T., Viukov, S., Manor, Y.S., Dietmann, S., Hanna, J.H., and Surani, M.A. (2015). SOX17 is a critical specifier of human primordial germ cell fate. Cell *160*, 253–268.

Kagiwada, S., Kurimoto, K., Hirota, T., Yamaji, M., and Saitou, M. (2013). Replication-coupled passive DNA demethylation for the erasure of genome imprints in mice. EMBO J. *32*, 340–353.

Kobayashi, H., Sakurai, T., Miura, F., Imai, M., Mochiduki, K., Yanagisawa, E., Sakashita, A., Wakai, T., Suzuki, Y., Ito, T., et al. (2013). High-resolution DNA methylome analysis of primordial germ cells identifies gender-specific reprogramming in mice. Genome Res. *23*, 616–627.

Kriaucionis, S., and Heintz, N. (2009). The nuclear DNA base 5-hydroxymethylcytosine is present in Purkinje neurons and the brain. Science *324*, 929–930.

Krueger, F., and Andrews, S.R. (2011). Bismark: a flexible aligner and methylation caller for Bisulfite-Seq applications. Bioinformatics *27*, 1571–1572.

Kubo, N., Toh, H., Shirane, K., Shirakawa, T., Kobayashi, H., Sato, T., Sone, H., Sato, Y., Tomizawa, S., Tsurusaki, Y., et al. (2015). DNA methylation and gene expression dynamics during spermatogonial stem cell differentiation in the early postnatal mouse testis. BMC Genomics *16*, 624.

Kurimoto, K., Yabuta, Y., Hayashi, K., Ohta, H., Kiyonari, H., Mitani, T., Moritoki, Y., Kohri, K., Kimura, H., Yamamoto, T., et al. (2015). Quantitative dynamics of chromatin remodeling during germ cell specification from mouse embryonic stem cells. Cell Stem Cell *16*, 517–532.

Lee, H.J., Hore, T.A., and Reik, W. (2014). Reprogramming the methylome: erasing memory and creating diversity. Cell Stem Cell *14*, 710–719.

Lister, R., Pelizzola, M., Dowen, R.H., Hawkins, R.D., Hon, G., Tonti-Filippini, J., Nery, J.R., Lee, L., Ye, Z., Ngo, Q.M., et al. (2009). Human DNA methylomes at base resolution show widespread epigenomic differences. Nature *462*, 315–322.

Lister, R., Pelizzola, M., Kida, Y.S., Hawkins, R.D., Nery, J.R., Hon, G., Antosiewicz-Bourget, J., O'Malley, R., Castanon, R., Klugman, S., et al. (2011). Hotspots of aberrant epigenomic reprogramming in human induced pluripotent stem cells. Nature *471*, 68–73.

Ma, Z., Swigut, T., Valouev, A., Rada-Iglesias, A., and Wysocka, J. (2011). Sequence-specific regulator Prdm14 safeguards mouse ESCs from entering extraembryonic endoderm fates. Nat. Struct. Mol. Biol. *18*, 120–127.

Miura, F., Enomoto, Y., Dairiki, R., and Ito, T. (2012). Amplification-free whole-genome bisulfite sequencing by post-bisulfite adaptor tagging. Nucleic Acids Res. *40*, e136.

Murakami, K., Gunesdogan, U., Zylicz, J.J., Tang, W.W., Sengupta, R., Kobayashi, T., Kim, S., Butler, R., Dietmann, S., and Surani, M.A. (2016). NANOG alone induces germ cells in primed epiblast in vitro by activation of enhancers. Nature *529*, 403–407.

Nakaki, F., Hayashi, K., Ohta, H., Kurimoto, K., Yabuta, Y., and Saitou, M. (2013). Induction of mouse germ-cell fate by transcription factors in vitro. Nature *501*, 222–226.

Okamoto, I., Otte, A.P., Allis, C.D., Reinberg, D., and Heard, E. (2004). Epigenetic dynamics of imprinted X inactivation during early mouse development. Science *303*, 644–649.

Peric-Hupkes, D., Meuleman, W., Pagie, L., Bruggeman, S.W., Solovei, I., Brugman, W., Graf, S., Flicek, P., Kerkhoven, R.M., van Lohuizen, M., et al. (2010). Molecular maps of the reorganization of genome-nuclear lamina interactions during differentiation. Mol. Cell *38*, 603–613.

Raddatz, G., Gao, Q., Bender, S., Jaenisch, R., and Lyko, F. (2012). Dnmt3a protects active chromosome domains against cancer-associated hypomethylation. PLoS Genet. *8*, e1003146.

Saitou, M., Kagiwada, S., and Kurimoto, K. (2012). Epigenetic reprogramming in mouse pre-implantation development and primordial germ cells. Development *139*, 15–31.

Sasaki, H., and Matsui, Y. (2008). Epigenetic events in mammalian germ-cell development: reprogramming and beyond. Nat. Rev. Genet. *9*, 129–140.

Sasaki, K., Yokobayashi, S., Nakamura, T., Okamoto, I., Yabuta, Y., Kurimoto, K., Ohta, H., Moritoki, Y., Iwatani, C., Tsuchiya, H., et al. (2015). Robust in vitro induction of human germ cell fate from pluripotent stem cells. Cell Stem Cell *17*, 178–194.

Schubeler, D. (2015). Function and information content of DNA methylation. Nature *517*, 321–326.

Schulz, E.G., Meisig, J., Nakamura, T., Okamoto, I., Sieber, A., Picard, C., Borensztein, M., Saitou, M., Bluthgen, N., and Heard, E. (2014). The two active X chromosomes in female ESCs block exit from the pluripotent state by modulating the ESC signaling network. Cell Stem Cell *14*, 203–216.

Seisenberger, S., Andrews, S., Krueger, F., Arand, J., Walter, J., Santos, F., Popp, C., Thienpont, B., Dean, W., and Reik, W. (2012). The dynamics of genome-wide DNA methylation reprogramming in mouse primordial germ cells. Mol. Cell *48*, 849–862.

Sharif, J., Muto, M., Takebayashi, S., Suetake, I., Iwamatsu, A., Endo, T.A., Shinga, J., Mizutani-Koseki, Y., Toyoda, T., Okamura, K., et al. (2007). The SRA protein Np95 mediates epigenetic inheritance by recruiting Dnmt1 to methylated DNA. Nature *450*, 908–912.

Shirane, K., Toh, H., Kobayashi, H., Miura, F., Chiba, H., Ito, T., Kono, T., and Sasaki, H. (2013). Mouse oocyte methylomes at base resolution reveal genome-wide accumulation of non-CpG methylation and role of DNA methyltransferases. PLoS Genet. *9*, e1003439.

Stadler, M.B., Murr, R., Burger, L., Ivanek, R., Lienert, F., Scholer, A., Wirbelauer, C., Oakeley, E.J., Gaidatzis, D., Tiwari, V.K., et al. (2011). DNA-binding factors shape the mouse methylome at distal regulatory regions. Nature *480*, 490–495.

Tahiliani, M., Koh, K.P., Shen, Y., Pastor, W.A., Bandukwala, H., Brudno, Y., Agarwal, S., Iyer, L.M., Liu, D.R., Aravind, L., et al. (2009). Conversion of 5-methylcytosine to 5-hydroxymethylcytosine in mammalian DNA by MLL partner TET1. Science *324*, 930–935.

Tang, W.W., Dietmann, S., Irie, N., Leitch, H.G., Floros, V.I., Bradshaw, C.R., Hackett, J.A., Chinnery, P.F., and Surani, M.A. (2015). A unique gene regulatory network resets the human germline epigenome for development. Cell *161*, 1453–1467.

Trapnell, C., Pachter, L., and Salzberg, S.L. (2009). TopHat: discovering splice junctions with RNA-Seq. Bioinformatics *25*, 1105–1111.

von Meyenn, F., Iurlaro, M., Habibi, E., Liu, N.Q., Salehzadeh-Yazdi, A., Santos, F., Petrini, E., Milagre, I., Yu, M., Xie, Z., et al. (2016). Impairment of DNA methylation maintenance is the main cause of global demethylation in naive embryonic stem cells. Mol. Cell *62*, 848–861.

Wang, L., Zhang, J., Duan, J., Gao, X., Zhu, W., Lu, X., Yang, L., Zhang, J., Li, G., Ci, W., et al. (2014). Programming and inheritance of parental DNA methylomes in mammals. Cell *157*, 979–991.

Weber, M., Hellmann, I., Stadler, M.B., Ramos, L., Paabo, S., Rebhan, M., and Schubeler, D. (2007). Distribution, silencing potential and evolutionary impact of promoter DNA methylation in the human genome. Nat. Genet. *39*, 457–466.

Yamaguchi, S., Shen, L., Liu, Y., Sendler, D., and Zhang, Y. (2013). Role of Tet1 in erasure of genomic imprinting. Nature *504*, 460–464.

Yamaji, M., Seki, Y., Kurimoto, K., Yabuta, Y., Yuasa, M., Shigeta, M., Yamanaka, K., Ohinata, Y., and Saitou, M. (2008). Critical function of Prdm14 for the establishment of the germ cell lineage in mice. Nat. Genet. *40*, 1016–1022.

Yamaji, M., Ueda, J., Hayashi, K., Ohta, H., Yabuta, Y., Kurimoto, K., Nakato, R., Yamada, Y., Shirahige, K., and Saitou, M. (2013). PRDM14 ensures naive pluripotency through dual regulation of signaling and epigenetic pathways in mouse embryonic stem cells. Cell Stem Cell *12*, 368–382.

Ying, Q.L., Wray, J., Nichols, J., Batlle-Morera, L., Doble, B., Woodgett, J., Cohen, P., and Smith, A. (2008). The ground state of embryonic stem cell self-renewal. Nature *453*, 519–523.

Zvetkova, I., Apedaile, A., Ramsahoye, B., Mermoud, J.E., Crompton, L.A., John, R., Feil, R., and Brockdorff, N. (2005). Global hypomethylation of the genome in XX embryonic stem cells. Nat. Genet. *37*, 1274–1279.